

Article

Near-Infrared, Light-Triggered, On-Demand Anti-Inflammatories and Antibiotics Release by Graphene Oxide/Electrospun PCL Patch for Wound Healing

Nicolò Mauro ^{1,2,*}, Salvatore Emanuele Drago ¹, Gennara Cavallaro ¹ and Gaetano Giammona ¹

¹ Laboratory of Biocompatible Polymers, Department of “Scienze e Tecnologie Biologiche, Chimiche e Farmaceutiche” (STEBICEF), University of Palermo, Via Archirafi, 32 90123 Palermo, Italy; salvatoreemanuele.drago@unipa.it (S.E.D.); gennara.cavallaro@unipa.it (G.C.); gaetano.giammona@unipa.it (G.G.)

² Fondazione Umberto Veronesi, Piazza Velasca 5, 20122 Milano, Italy

* Correspondence: nicolo.mauro@unipa.it; Tel./Fax: +39-09123891928

Received: 23 September 2019; Accepted: 19 October 2019; Published: 23 October 2019



Abstract: Very recently, significant attention has been focused on the adsorption and cell adhesion properties of graphene oxide (GO), because it is expected to allow high drug loading and controlled drug release, as well as the promotion of cell adhesion and proliferation. This is particularly interesting in the promotion of wound healing, where antibiotics and anti-inflammatories should be locally released for a prolonged time to allow fibroblast proliferation. Here, we designed an implantable patch consisting of poly(caprolactone) electrospun covered with GO, henceforth named GO-PCL, endowed with high ibuprofen (5.85 mg cm^{-2}), ketoprofen (0.86 mg cm^{-2}), and vancomycin (0.95 mg cm^{-2}) loading, used as anti-inflammatory and antibiotic models respectively, and capable of responding to near infrared (NIR)-light stimuli in order to promptly release the payload on-demand beyond three days. Furthermore, we demonstrated the GO is able to promote fibroblast adhesion, a key characteristic to potentially provide wound healing in vivo.

Keywords: on-demand drug release; graphene oxide; plasma; polycaprolactone; vancomycin; wound healing

1. Introduction

Under certain circumstances, such as burns and chronic skin conditions, wound healing processes can be jeopardized by inflammation and infections [1,2]. Regions of avascularization, necrosis, prolonged and increased inflammation, and inability of immune-cells to avoid bacterial infections are all critical challenges inhibiting the physiologic healing of chronic wounds [1]. In particular, intense inflammation affects the expression of metalloproteinase MMPs, thereby reducing important mechanisms of wound repair, such as extracellular matrix (ECM) remodeling. Furthermore, bacterial infections could lead to biofilm, which further enhances inflammation, inhibiting ECM deposition and tissue repair.

Smart wound bandages should primarily aim to prevent bacterial infection by adequate covering of the wound microenvironment from external contaminants. On the other hand, they should be able to inhibit tissue hyperinflammation and provide cell proliferation so as to promote tissue regeneration [2,3]. Therefore, materials used in the treatment of burn or skin conditions are employed as scaffold to host endogenous cells and facilitate their growth in situ, and as biodegradable bandage to protect the wound area and simultaneously keep suitable conditions to support the healing process. The ideal scaffold is

supposed to be biocompatible, preserve water content in order to prevent dehydration, and permit oxygenation of the growing tissue without interfering with the wound healing [4,5]. Furthermore, it should display a degradation kinetic comparable to the rate of tissue growth, thus promoting a rapid healing process while it degrades [6].

Taking this in mind, engineered polymeric scaffolds have been recently developed to create three-dimensional architecture that can mimic the ECM and allow in situ tissue regeneration. In particular, electrospun patches with micro and nanofiber architectures obtained by electrospinning of polyesters, such as polylactic acid (PLA) and poly(caprolactone) (PCL), yield to scaffolds able to mimic the natural collagen fibers in ECM [2,7]. Because of the crucial role of collagen fibers in maintaining the integrity of skin, electrospun polymeric patches are attracting biomimetic materials potentially able to provide wound healing in vivo [2,6]. Additionally, electrospinning is a mild technique that allows loading of bioactive molecules, such as antibiotics or nonsteroidal anti-inflammatory drugs, to equip the final patch with additional pharmacological effects useful to maintain a suitable environment for skin regeneration [8,9]. Moreover, materials able to release their cargo on-demand have attracted interest from scientists, so as to keep the wound healing processes for a prolonged time and only if required. Thus, plenty of on-demand release biomaterials were prepared involving different mechanisms to trigger drug release, such as stimulus-sensitive hydrogels and polymeric drug loaded nanospheres [10–12]. However, a multiple drug loaded and bioresorbable patch that possesses on-demand antibiosis and anti-inflammatory abilities still has not been achieved, which would have great potential in skin regeneration applications.

Herein, to address this issue, we report on an effective and industrially scalable approach to obtain a composite highly biodegradable patch with near infrared (NIR)-triggered antimicrobial and anti-inflammatory properties and cell proliferation ability, so as to promote wound healing through graphene oxide (GO) covalently deposited onto a PCL scaffold. Indeed, GO exhibits multifunctional properties that are useful in drug delivery applications, including enhancement of drug loading owing to the huge surface area and on-demand electrical/near infrared (NIR)-triggered drug release in the site of action [13–18]. In addition, GO coating has been proposed as a cell adhesion and proliferation promoter through nonspecific interaction with living cells [19,20]. We sought to exploit a previously developed hybrid patch consisting of PCL electrospun, an FDA approved material [21], covered with GO in order to obtain a composite patch endowed with high nonsteroidal anti-inflammatory drugs and antibiotics loading capability, and capable of responding to NIR-light stimuli in order to promptly release the payload on-demand for a prolonged time. Furthermore, we try to demonstrate that GO can promote fibroblast adhesion and proliferation while guaranteeing a suitable degradation rate, a characteristic to potentially provide wound healing in vivo. We show low-vacuum, plasma-assisted GO covalent deposition as a potential technology for the surface functionalization of biomaterials with GO sheets for on-demand antimicrobial and anti-inflammatory actions, combined with in situ cell proliferation ability, to promote wound healing in skin conditions.

2. Materials and Methods

2.1. Materials

Poly(caprolactone), dichloromethane (DCM), N,N-dimethylformamide (DMF), and Dulbecco's phosphate buffer solution (DPBS) were purchased from Sigma Aldrich (Milan, Italy). Graphene oxide nanosheets (1 nm thickness, 500 nm width) were purchased from ACS Material, LLC, Pasadena, CA, USA. O₂ (99.5%) and N₂ (99.8%) were purchased from Air Liquide Italia Service Srl. Dulbecco's minimum essential medium (DMEM) was purchased from Euroclone. Celltracker green[®] and Celltraker Cy5[®] 4',6-diamidino-2-phenylindole (DAPI) were purchased from Life Technologies (Waltham, MA, USA).

Human dermal fibroblast cells (HDFa) (obtained from Life Technologies, Waltham, MA, USA) were maintained in Dulbecco's modified eagle medium (DMEM) containing 10% (*v/v*) fetal bovine serum

(FBS, Euroclone, Milan, Italy), 100 units per mL penicillin G, 100 $\mu\text{g mL}^{-1}$ streptomycin (Euroclone), and 2 mM L-glutamine (Euroclone, Celbar) at 37 °C, in a humidified atmosphere of 5% CO_2 .

2.2. Scaffold Preparation

PCL were prepared using widespread electrospinning [22,23]. PCL patch (380 mg, $\approx 21 \text{ cm}^2$, $\approx 600 \mu\text{m}$ thickness) was then placed in a low pressure plasma reactor (FEMTO, Diener Electronic Plasma-Surface-Technology, Ebhausen, GmbH) and treated for 10 min: 40 kHz; 1 W; N_2 15 sccm; 1.0 mbar. The activation was carried out using nitrogen plasma. Then, the activated patch was immediately soaked in a sealed petri dish containing an aqueous solution of graphene oxide nanosheets pH 10 (0.5 mg mL^{-1}). The reaction was maintained at 37 °C for 48 h under continuous stirring (150 rpm) in a Benchtop 808C Incubator Orbital Shaker model 420. The scaffolds were finally washed-up using milliQ water ($5 \times 200 \text{ mL}$), washed with water over night (200 mL), and dried (0.1 Torr). The efficiency of GO conjugation was calculated on a weight basis (3.6% *w/w*).

2.3. Attenuated Total Reflectance Infrared Spectroscopy (FTIR-ATR)

The Fourier transform infrared spectra (FTIR) were recorded in the range of 400–4000 cm^{-1} with 32 scans and 4 cm^{-1} resolution, using an ATR accessory in a Bruker Alpha FTIR spectrometer.

2.4. X-ray Photoelectron Spectroscopy (XPS)

The XPS spectra of PCL and GO–PCL were recorded on a PHI 5000 VersaProbeII (ULVAC-PHI, Inc, Kanagawa, Japan); source: $\text{K}\alpha$, 1486.6 eV; beam: 200 μm , 50 W; time per step: 10 ms; energy step: 0.10 eV; pass energy: 23.50 eV; analyzer mode: FAT. Both samples were dried under vacuum (0.1 Torr) for 24 h before the analyses. The carbon (C 1s) line at 284.8 eV was used as reference energy.

2.5. Scanning Electron Microscopy (SEM)

Morphological characteristics of GO–PCL were evaluated by a scanning electron microscope (FEI ESEM Quanta200, Graz, GmbH) operating at 10 kV. The sample was deposited onto a carbon-coated steel stub, dried under vacuum (0.1 Torr), and sputter-coated with gold (15 nm thickness) prior to microscopy examination.

2.6. Water Uptake

Percentage water uptake of scaffolds was determined in water, on scaffolds 800 μm in thickness and with a base diameter of 50 mm [24]. All samples were dried to constant weight at 0.1 Torr, before being put into a test tube containing 50 mL of milliQ water maintained at 37 °C. The disc was retrieved, gently wiped with soft filter paper, and weighed. Maximum water uptake was observed after about 4 h. The reported values were the average of 6 experiments with a percent mean variation coefficient, CV%, lower than 5%.

2.7. Degradation Time

Degradation kinetics was observed by following the weight loss of the scaffolds maintained at 37 °C in PBS pH 7.4 (50 mL) up to 12 months from incubation [25,26]. All samples were dried to constant weight and placed in a test tube containing the degradation medium. The weight loss was measured at scheduled time intervals. In particular, the samples were retrieved, gently wiped with soft filter paper, and weighed. All experiments were performed in triplicate ($n=9$, 3 independent replicates). In all tests the mean CV% was $< 5\%$.

2.8. Water Contact Angle Measurement

The hydrophilicity of electrospun PCL patches was studied by a video contact angle instrument (VCA Optima, AST Products, Inc, Billerica, MA, USA). Deionized water was dropped onto the surface

of the fibrous scaffold, and an image of the drop was recorded. The VCA Optima software was used to calculate the contact angle.

2.9. Drug Loading and Drug Release Kinetics

The PCL-GO patch (1 cm²) was put into a test tube containing an aqueous solution of either sodium ketoprofen, sodium ibuprofen, or vancomycin hydrochloride (1.5 mL, 7% *w/v*), and kept for 15 hours at 37 °C in an orbital shaker (100 rpm). After that, each patch was washed with ultrapure water, and aqueous waste was added to the residual volume of the free drug solution, while patches were dried under vacuum (0.75 Torr) for 3 days. To determine the amount of the adsorbed drug, the residual drug solution was diluted up to 5 mL, and the amount of free drug was quantified spectrophotometrically using calibration curves made of drug standards: $\lambda_{\text{ibuprofen}} = 264$; $\lambda_{\text{ketoprofen}} = 260$; $\lambda_{\text{vancomycin}} = 280$.

For the drug release study, the PCL-GO patch (4.95 cm²: 4.22, 28.72 and 4.66 mg of Ketoprofen, Ibuprofen, or Vancomycin, respectively) was placed onto a Franz cell (25mm orifice, 20 mL acceptor compartment volume, 4.91 cm² donor compartment area) donor compartment and fixed at the perimeter using an o ring silicon seal. Then, 20 mL of PBS pH 7.4 was added to the acceptor compartment, kept at 37 °C under continuous stirring. A quantity of 1 mL of solution was withdrawn from the acceptor compartment at scheduled time intervals and replaced with equal amount of fresh medium. The amount of drug released was evaluated spectrophotometrically, evaluating the absorbance of each sample as above reported, and using the ϵ obtained from standard solutions of the drugs in the same medium. Then, the cumulative release was determined as a function of incubation time. In a parallel experiment, the NIR-triggered photothermal drug release was evaluated, treating the patch with an 810 nm laser diode (power fitted at 5 W cm⁻²) for 200 s and evaluating the pulsed release over time. The on-demand NIR-triggered release was assessed five times to establish the feasibility of a pulsed release over time. Each experiment was carried out in triplicate, and the results were in agreement within $\pm 5\%$ standard error.

2.10. Cell Adhesion Assay

Cell adhesion and proliferation on the virgin, nitrogen plasma activated and GO functionalized patches, namely, PCL, PCL-N₂, and GO-PCL, respectively, were evaluated by MTS assay, after incubation with human dermal fibroblast cells (HDFa) (Life Technologies) for 24 h. The scaffolds were placed at the bottom of a 48-multiwell plate using plate insert (CellCrownTM48, Sigma Aldrich), and cells (5×10^4 cells/well) were seeded on scaffolds and grown in DMEM. After 24 h, patches were withdrawn, washed twice with DPBS, and placed into clean well plates before performing the MTS assay. A fresh MTS solution in DMEM was added to each well (400 μ L), and cells were incubated for additional 3 h. The absorbance at 492 nm was measured using a microplate reader (Plate Reader AF2200, Eppendorf). Seeded cells, as they were, were used for the MTS assay as reference control.

2.11. Statistical Analysis

Data are presented as mean \pm s.e.m., and p-values were determined using a Siegel–Tukey test for single comparisons. Statistical analysis was performed using Statext online software.

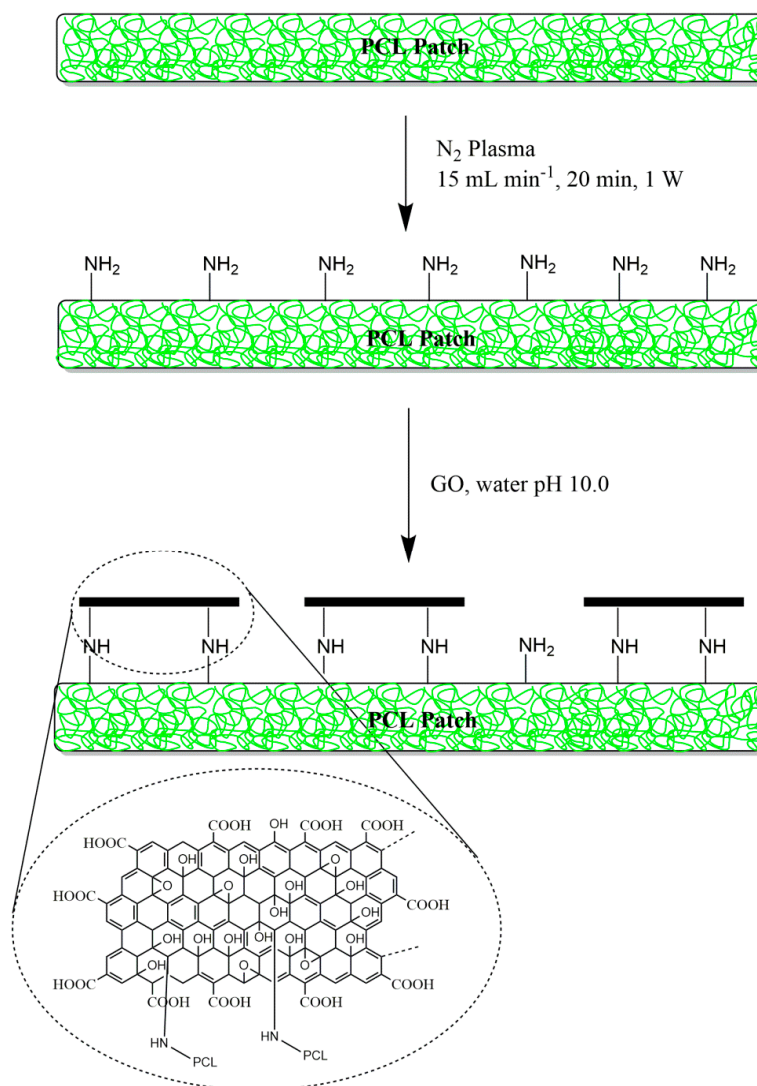
3. Results and Discussion

3.1. Surface Functionalization of PCL Patch with GO Via Nonthermal Low-Vacuum Nitrogen Plasma

This work reports the development of an electrospun PCL patch, functionalized with GO via nitrogen plasma activation, for the on-demand release of nonsteroidal anti-inflammatory and antibiotic drugs by means of NIR-light stimuli. Furthermore, this nanocomposite material could be exploited as a wound healing promoter, because of their cell adhesion and proliferation properties [23,27].

This patch is designed to be potentially employed as a scaffold for the protract treatment of injuries and burns so as to prevent inflammation and bacterial contamination, and provide suitable tissue

regeneration *in vivo*. This was accomplished by tuning the electrospun PCL physicochemical surface features through low-vacuum nitrogen plasma activation and GO covalent functionalization (Scheme 1). In particular, PCL patches (6 μm fiber diameter, surface $2 \times 21 \text{ cm}^2$, $\approx 600 \mu\text{m}$ thickness) were employed as polymeric scaffold, as they are mechanically robust, biodegradable, and biocompatible. The surface functionalization involved two-step tandem reactions. In a first step, PCL patches were treated with low-vacuum nitrogen plasma, just enough to activate the microfiber surface with amine functions while still preserving the bulk microstructures. In fact, corrosion of the polymeric surface could occur, and this might affect the 3D macrostructure of the PCL scaffold. This approach has been successfully used for scaffold engineering to provide functionalization of the surface with primary amines, even if keeping bulk properties of the virgin polymeric material, and also to enhance cell adhesion properties of hydrophobic polymers [22,28–30]. Furthermore, primary amines also allow monolayer covalent deposition of GO through the reaction with epoxy groups intrinsically contained in GO sheets [31]. GO consists of single graphitic monolayer with randomly distributed aromatic regions (sp_2 carbon atoms) and oxygenated aliphatic regions (sp_3 carbon atoms) containing hydroxyl, epoxy, carbonyl, and carboxyl functional groups. Hence, GO was functionalized with aliphatic amines on the PCL surface under slightly basic conditions and without perturbing its main structure because of versatile chemistry of epoxy groups [23,32].



Scheme 1. Synthetic steps involved in the surface functionalization of poly(caprolactone) (PCL) microfibers with graphene oxide (GO).

The morphological characterization of the hybrid patch by scanning electron microscopy (SEM) revealed that microfibers did not undergo significant corrosion phenomena, but they were stably covered by GO sheets (Figure 1a,a'). Better yet, some GO sheets were able to bridge the gap between different microfibers, perhaps due to covalent bonds established with different amine groups (Figure 1a').

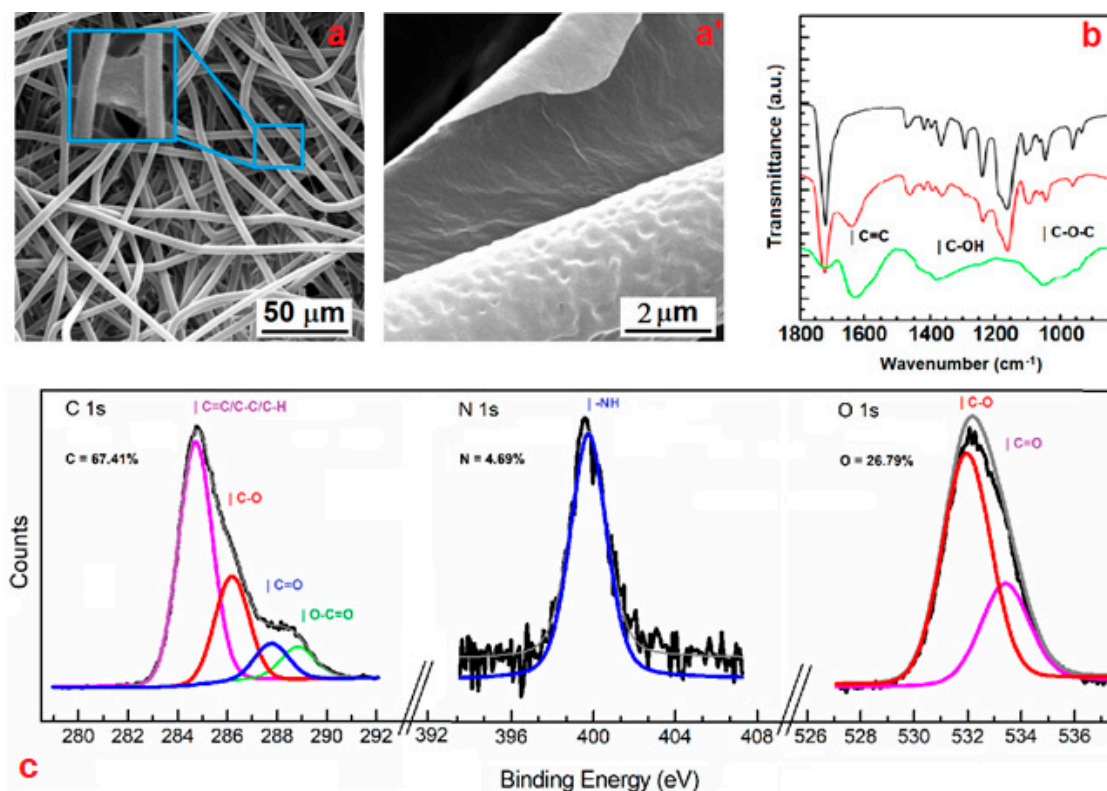


Figure 1. SEM analysis (a,a') of the GO-PCL sample. Fourier transform infrared (FTIR) spectra of PCL (black), GO-PCL (red), and GO (green) in the region within 1800–800 cm^{-1} (b). X-ray photoelectron spectroscopy (XPS) spectrum of GO-PCL: experimental spectrum (black), composite spectrum (grey), and deconvolution peaks are showed as colored curves (c).

The GO deposition onto the patch surface was confirmed by FTIR spectroscopy. Spectra in the region 1800–800 cm^{-1} are presented in Figure 1b. The vibration band observed at 1749, 1611, and 1667 cm^{-1} , ascribable to the C=O, asymmetric COO^- , and C=C stretching, respectively, indicates the presence of GO sheets at the patch surface. In addition, the same modes of vibration of the bulk PCL were observed in the GO-PCL, such as those at 2916–2970 and 1724 cm^{-1} , attributable to C–H and C=O stretching, pointing out that the functionalization with GO took place at the patch microfiber surface. Moreover, it might be noticed that a sharp decrease of the typical bands located at 1040 cm^{-1} , corresponding to the epoxy (C–O–C) stretching mode over the basal plane of GO skeleton, hints that the functionalization of PCL with GO involved the reaction with epoxy functions. The low amount of GO sheets revealed by FTIR spectroscopy and the reaction yield (3.6% on a weight basis) also confirmed that GO deposition occurred only at the microfiber surface.

The covalent nature of these bonds was also confirmed by means of X-ray photoelectron spectroscopy (XPS). Figure 1c shows the typical peaks of the XPS spectrum and the elemental composition for the GO-PCL. XPS analysis obtained after nitrogen plasma activation showed diagnostic peaks of GO in the C 1s core level. In particular, the characteristic peaks related to the C=C and C=O bonds in GO (284.7 and 287.8 eV, respectively) can be distinguished in the C 1s core level. Furthermore, a remarkable peak at 399.2 eV in the N 1s core level region was observed, indicating the efficient derivatization of the patch with prim- or sec- amine groups. In agreement with FTIR data, this peak

entails that the functionalization of the microfibers with GO involved the nucleophilic attack of reactive primary amine functions to the epoxy groups of the GO sheets.

3.2. GO Allows Water Uptake and Accelerates Degradation of the Scaffold

Plasma-induced covalent GO coating can affect the physicochemical properties of the PCL patch in terms of biodegradability and water uptake, as hydroxyl, carboxyl, and amine groups introduced at the material/medium interface improve the hydrophilicity of the patch surface. Water uptake is an important feature of biomaterials, which are designed to be somehow placed in the body (e.g., patches for regenerative applications and implants). This, because of a high water content, reduces interfacial tensions between the biomaterial and surrounding tissues, thus limiting inflammation [33].

The water uptake observed in water for the plasma activated scaffold (PCL-N₂) was 5.4 times higher than that of the virgin PCL patch (Figure 2a), while the water uptake observed for the GO-PCL patch was about six times higher, entailing a significant effect of the GO coating on water uptake, owing to its high water permeability [34].

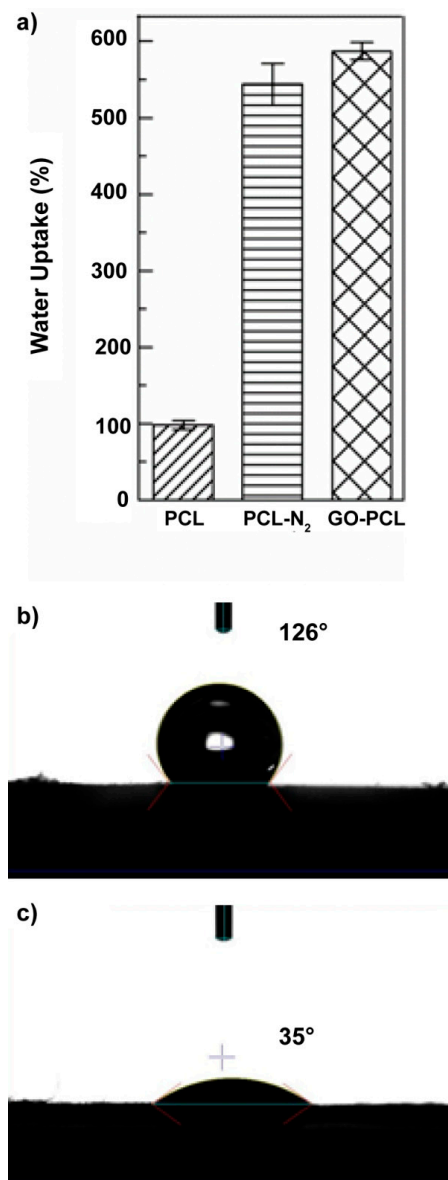


Figure 2. Water uptake (a) and water contact angle measurements for the virgin PCL (b) and GO-PCL patches (c).

Another factor that strongly influences the biomaterial/tissue interface is the wettability in aqueous media. To optimize the biocompatibility and the adhesion and properties of the patch in order to promote wound healing, the rule is “the higher the better” [35]. With this in mind, we performed water contact angle measurements for GO–PCL patches and compared these with that of the virgin PCL (Figure 2b,c). The contact angle of the bare PCL was beyond 120° (Figure 2b), implying a scarce water wettability, whereas the functionalized PCL patch displayed very low values (~35°), which indicate high wettability in physiological media (Figure 2c).

These data suggest on the whole that the functionalization of the PCL patch with GO sheets improves its surface performance toward physiological interfaces, which it might expect to affect the biocompatibility and cell adhesion properties.

Water uptake and wettability can also play a part in determining degradation of the PCL patch, as it mainly occurs by hydrolysis. Thus, the degradation kinetic of the GO–PCL was assessed and compared to that of the bare PCL patch (Figure 3) [36]. It may be noticed that the degradation of the functionalized patch is time-dependent and shorter to that observed for the bare patch (~ 12 vs >> 12 months, respectively). In particular, for the bare PCL patch, only 21% of weight loss was observed after 12 months of incubation at 37 °C (Figure 3). The higher degradation rate observed for the functionalized patch suggests that GO endows microfibers with hydrophilic groups, which allow surface reorientation and subsequent higher water diffusion at the biomaterial/medium interface [37]. This is proof that GO functionalization involves the formation of covalent bonds at the PCL surface.

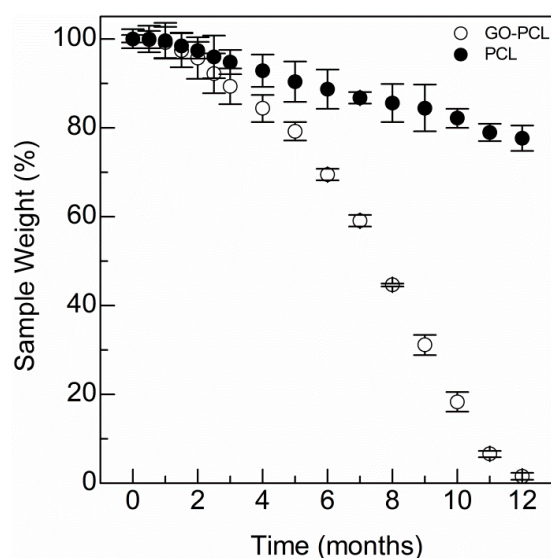


Figure 3. Degradation kinetics of the GO–PCL patch compared with the virgin PCL sample.

3.3. GO Coating Improves the Drug Loading and can Promote On-Demand Drug Release

The GO–PCL patch was designed to locally release a controlled amount of nonsteroidal anti-inflammatory drugs (i.e., ibuprofen and ketoprofen) and antibiotics (vancomycin), which could be used as on-demand treatment for burns and skin conditions [38]. This was accomplished by NIR-light external stimulus, which implies advantages for several reasons including biocompatibility, high temporal control, ease of use, and its noninvasive nature. Here, NIR light was absorbed by GO sheets at the GO–PCL surface, to be dissipated via vibrational motion affording local heating and, consequently, drug release. However, the rule of GO is manifold. Apart from the NIR-triggered on-demand release, it was employed for its outstanding ability to adsorb high amounts of hydrophobic drugs. In fact, GO–PCL was able to load a high amount of ketoprofen, ibuprofen, and vancomycin, used as model drugs, by means of simple immersion in drug solution (Table 1). In particular, drug loading observed for the GO–PCL patch was about 6.5–3 times higher compared with common commercially available patches (Table 1). This could provide suitable treatments for a prolonged time.

Table 1. Drug loading of GO–PCL compared with commercially available patches.

Sample	Ketoprofen ^a (mg/cm ²)	Ibuprofen ^a (mg/cm ²)	Vancomycin ^a (mg/cm ²)
GO–PCL	0.86 ± 0.01	5.85 ± 0.13	0.95 ± 0.05
Keplant [®]	0.29 ± 0.02	n.a.	n.a.
Ibupas [®]	n.a.	0.89 ± 0.08	n.a.

^a Drug loading obtained by UV spectrophotometry.

Drug release studies reported in Figure 4 show that GO–PCL slowly released the drug payload without hinting to a burst effect, thus suggesting that there is no sponge-like physical absorption of drugs into the patch. Indeed, a sharp release of active therapeutics from the surface occurred only after NIR light was shined onto the surface. The NIR-triggered on-demand drug release from the GO–PCL patch was studied using bicompartimental Franz cells in PBS pH 7.4, applying an 810 nm laser diode impulse for 200 s at scheduled time intervals (Figure 4a). An NIR exposure with low power density (5 Wcm^{-2}) was selected on the basis of a previously reported study, in order to avoid any harmful effects on skin cells [23]. The NIR-triggered drug release profiles were compared with those obtained without external stimulus (Figure 4b–d). GO–PCL released about 5% of its ketoprofen payload after 70 h of incubation, while under cyclic NIR-light stimulus it was able to release up to 23% of ketoprofen within the same time interval (Figure 4b), releasing about 4% of the ketoprofen payload whenever it is applied the light irradiation. A similar trend, although more moderate, was observed for ibuprofen (Figure 4c).

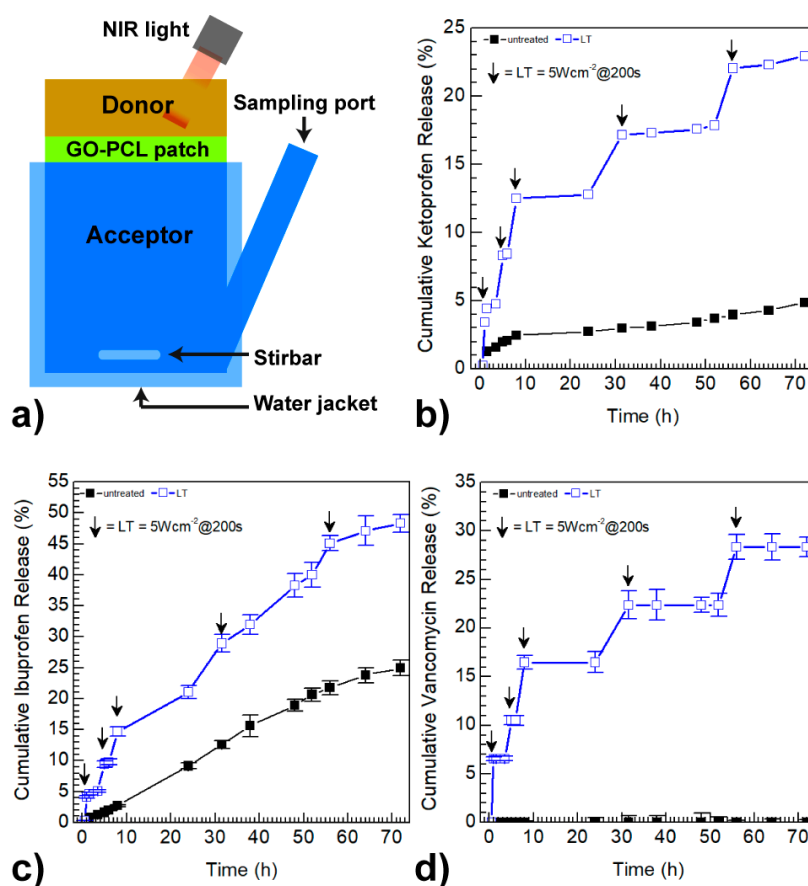


Figure 4. Schematization of a Franz cell used for drug release studies (a). Ketoprofen (b), ibuprofen (c) and vancomycin (d) release profiles of the drug loaded GO–PCL patches in PBS pH 7.4 after five cycles of near infrared (NIR) photo-stimulation: each arrow indicates the exposure to an 810 nm laser diode for 200 s and a power density of 5 Wcm^{-2} .

A remarkable NIR-light-dependent release was observed for vancomycin (Figure 4d). Whilst no vancomycin release was observed without NIR stimulus, GO-PCL released beyond 28% of the vancomycin payload over the entire range considered. This could be ascribed to the higher aromatic character of vancomycin, which results in the formation of stable π - π stacking interactions with GO. Overall, each NIR-light impulse activates the release of about 4–6% of the drug payload, confirming that GO coating plays a crucial role in determining a suitable on-demand release in situ.

3.4. GO Can Foster Wound Healing by Improving Cell Adhesion and Proliferation

Here, GO functionalization onto PCL microfibers was achieved for various reasons. On the one hand, if the PCL patch does not have enough available specific surface, it would not be able to load a high quantity of drugs to be released in situ. In addition, GO is able to trigger the release of drugs by selective NIR photo stimulation by producing local heat (phototherapy), and thus it was selected to obtain on-demand release of anti-inflammatory and antibiotic drugs at the wound site. On the other hand, GO has been recently studied as a cell adhesion and proliferation promoter owing to their hydrophilic and protein adsorption properties, which could be of help to provide wound healing during the pharmacological therapy [23,39,40].

An in vitro model of human fibroblasts (HDFa) was employed, as it is important to understand HDFa behavior within the skin in the context of wound healing [41,42].

HDFa cells were incubated on the top of the GO-PCL patches for 24 h, and then cell viability was quantified by MTS assay and compared to that observed for the bare PCL patch (Figure 5). Cell viability tests demonstrated the ability of GO-PCL to promote fibroblasts adhesion and proliferation in comparison with the bare patch (Figure 5). HDFa adhered at the GO-PCL surface up to about 80%, 16% higher than the value observed for the PCL patch (Figure 5). The adhesion factor, expressed as the $\text{Abs}_{492\text{nm}}^{24\text{h, sample}} / \text{Abs}_{492\text{nm}}^{24\text{h, control}}$ ratio, was roughly 1.25 times higher for the GO functionalized patch.

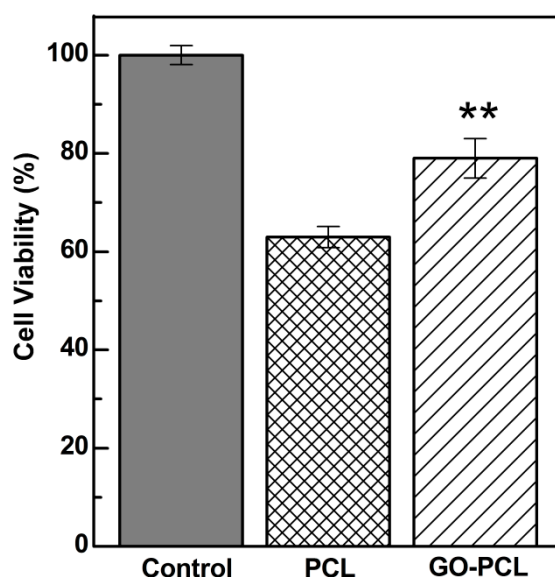


Figure 5. MTS assay after 24 h of incubation of the scaffolds with HDFa. Cell adhesion values are calculated comparing cell viability on each scaffold to that obtained for the free well (positive control). Data shown as mean \pm s.e.m. (n=6, two independent biological replicates); **P<0.01 (Siegel–Tukey test).

Given the importance of HDFa in fostering wound healing, one can assume that GO-PCL could be employed as a versatile scaffold to simultaneously activate self-repairing mechanisms of tissues in vivo,

and to provide suitable on-demand anti-inflammatory and antibiotic therapies to avoid undesired responses and infections.

4. Conclusions

Here, we designed an implantable patch consisting of poly(caprolactone) electrospun covered with GO, namely GO-PCL, to allow skin wound healing by combining on-demand release of nonsteroidal anti-inflammatory and antibiotic drugs with in situ fibroblast cell recruiting and proliferation. The surface covalent functionalization with GO, thanks to its huge surface area and outstanding adsorption properties, endows common polymeric patches with high ibuprofen (5.85 mg cm^{-2}), ketoprofen (0.86 mg cm^{-2}), and vancomycin (0.95 mg cm^{-2}) loading, used as anti-inflammatory and antibiotic models, respectively. Moreover, the immobilized GO sheets proved capable of responding to NIR-light stimuli, in order to promptly release the payload on-demand beyond three days. We also demonstrated that GO is able to promote fibroblast adhesion and proliferation, a key characteristic to potentially provide wound healing in vivo. Thus, we conclude that the functionalization of electrospun polymeric patches with GO described herein is a versatile, mild, cost effective, and scalable strategy that can be employed to prepare smart nanocomposite patches in the treatment of burns and skin conditions.

Author Contributions: N.M. conceived the project, performed reactions needed to produce functionalized patches, carried out drug release studies, analyzed results and wrote the main manuscript, S.E.D. performed the drug loading experiments and helped to write the manuscript, G.C. helped to write and revised the final manuscript, G.G. revised the final manuscript and led the main project.

Funding: This research was funded by Fondazione Umberto Veronesi, grant number FUV2019.

Acknowledgments: This work was supported by the Fondazione Umberto Veronesi (FUV Fellowship 2019).

Conflicts of Interest: The authors declare no conflict of interest.

References

1. Mustoe, T.A.; O'Shaughnessy, K.; Kloeters, O. Chronic wound pathogenesis and current treatment strategies: A unifying hypothesis. *Plast. Reconstr. Surg.* **2006**, *117*, 35S–41S. [[CrossRef](#)]
2. Saghazadeh, S.; Rinoldi, C.; Schot, M.; Kashaf, S.S.; Sharifi, F.; Jalilian, E.; Nuutila, K.; Giatsidis, G.; Mostafalu, P.; Derakhshandeh, H.; et al. Drug delivery systems and materials for wound healing applications. *Adv. Drug Deliv. Rev.* **2018**, *127*, 138–166. [[CrossRef](#)]
3. Vuerstaek, J.D.D.; Vainas, T.; Wuite, J.; Nelemans, P.; Neumann, M.H.A.; Veraart, J.C.J.M. State-of-the-art treatment of chronic leg ulcers: A randomized controlled trial comparing vacuum-assisted closure (V.A.C.) with modern wound dressings. *J. Vasc. Surg.* **2006**, *44*, 1029–1037. [[CrossRef](#)] [[PubMed](#)]
4. Wang, H.M.; Chou, Y.T.; Wen, Z.H.; Wang, Z.R.; Chen, C.H.; Ho, M.L. Novel Biodegradable Porous Scaffold Applied to Skin Regeneration. *PLoS ONE* **2013**, *8*, e56330. [[CrossRef](#)] [[PubMed](#)]
5. Boyce, S.T.; Lalley, A.L. Tissue engineering of skin and regenerative medicine for wound care. *Burns Trauma* **2018**, *6*, 4. [[CrossRef](#)]
6. Mele, E. Electrospinning of natural polymers for advanced wound care: Towards responsive and adaptive dressings. *J. Mater. Chem. B.* **2016**, *4*, 4801–4812. [[CrossRef](#)]
7. Chandrasekaran, A.R.; Venugopal, J.; Sundarajan, S.; Ramakrishna, S. Fabrication of a nanofibrous scaffold with improved bioactivity for culture of human dermal fibroblasts for skin regeneration. *Biomed. Mater.* **2011**, *6*, 015001. [[CrossRef](#)]
8. Huang, C.H.; Chi, C.Y.; Chen, Y.S.; Chen, K.Y.; Chen, P.L.; Yao, C.H. Evaluation of proanthocyanidin-crosslinked electrospun gelatin nanofibers for drug delivering system. *Mater. Sci. Eng. C* **2012**, *32*, 2476–2483. [[CrossRef](#)]
9. Ye, K.; You, M.; Mo, X. Electrospun Nanofibers for Tissue Engineering with Drug Loading and Release. *Pharmaceutics* **2019**, *11*, 182. [[CrossRef](#)] [[PubMed](#)]
10. Linsley, C.S.; Wu, B.M. Recent advances in light-responsive on-demand drug-delivery systems. *Ther. Deliv.* **2017**, *8*, 89–107. [[CrossRef](#)]
11. Prausnitz, M.R.; Mitragotri, S.; Langer, R. Current status and future potential of transdermal drug delivery. *Nat. Rev. Drug Discov.* **2004**, *3*, 115–124. [[CrossRef](#)]

12. Mostafalu, P.; Kiaee, G.; Giatsidis, G.; Khalilpour, A.; Nabavinia, M.; Dokmeci, M.R.; Sonkusale, S.; Orgill, D.P.; Tamayol, A.; Khademhosseini, A. A Textile Dressing for Temporal and Dosage Controlled Drug Delivery. *Adv. Funct. Mater.* **2017**, *27*, 1702399. [[CrossRef](#)]
13. Fiorica, C.; Mauro, N.; Pitarresi, G.; Scialabba, C.; Palumbo, F.S.; Giammona, G. Double-Network-Structured Graphene Oxide-Containing Nanogels as Photothermal Agents for the Treatment of Colorectal Cancer. *Biomacromolecules* **2017**, *18*, 1010–1018. [[CrossRef](#)]
14. Mauro, N.; Li Volsi, A.; Scialabba, C.; Licciardi, M.; Cavallaro, G.; Giammona, G. Photothermal ablation of cancer cells using folate-coated gold/grapheme oxide composite. *Curr. Drug Deliv.* **2017**, *14*, 433–443. [[CrossRef](#)] [[PubMed](#)]
15. Mauro, N.; Scialabba, C.; Cavallaro, G.; Licciardi, M.; Giammona, G. Biotin-containing reduced graphene oxide-based nanosystem as a multieffect anticancer agent: Combining hyperthermia with targeted chemotherapy. *Biomacromolecules* **2015**, *16*, 2766–2775. [[CrossRef](#)]
16. Huang, C.; Wu, J.; Jiang, W.; Liu, R.; Li, Z.; Luan, Y. Amphiphilic prodrug-decorated graphene oxide as a multi-functional drug delivery system for efficient cancer therapy. *Mater. Sci. Eng. C* **2018**, *89*, 15–24. [[CrossRef](#)]
17. Tiwari, H.; Karki, N.; Pal, M.; Basak, S.; Verma, R.K.; Bal, R.; Kandpal, N.D.; Bisht, G.; Sahoo, N.G. Functionalized graphene oxide as a nanocarrier for dual drug delivery applications: The synergistic effect of quercetin and gefitinib against ovarian cancer cells. *Colloids Surf. B Biointerfaces* **2019**, *178*, 452–459. [[CrossRef](#)] [[PubMed](#)]
18. Weaver, C.L.; Larosa, J.M.; Luo, X.; Cui, X.T. Electrically controlled drug delivery from graphene oxide nanocomposite films. *ACS Nano* **2014**, *8*, 1834–1843. [[CrossRef](#)]
19. Chang, S.-J.; Hyun, M.S.; Myung, S.; Kang, M.-A.; Yoo, J.H.; Lee, K.G.; Choi, B.G.; Cho, Y.; Park, G.L.J. Graphene growth from reduced graphene oxide by chemical vapour deposition: Seeded growth accompanied by restoration. *Sci. Rep.* **2016**, *6*, 22653. [[CrossRef](#)]
20. Chung, C.; Kim, Y.-K.; Shin, D.; Ryoo, S.-R.; Hong, B.H.; Min, D.-H. Biomedical Applications of Graphene and Graphene Oxide. *Acc. Chem. Res.* **2013**, *46*, 2211–2224. [[CrossRef](#)]
21. Koepsell, L.; Zhang, L.; Neufeld, D.; Fong, H.; Deng, Y. Electrospun Nanofibrous Polycaprolactone Scaffolds for Tissue Engineering of Annulus Fibrosus. *Macromol. Biosci.* **2011**, *11*, 391–399. [[CrossRef](#)] [[PubMed](#)]
22. Gualandi, C.; Bloise, N.; Mauro, N.; Ferruti, P.; Manfredi, A.; Sampaolesi, M.; Liguori, A.; Laurita, R.; Gherardi, M.; Colombo, V.; et al. Poly-L-Lactic Acid Nanofiber-Polyamidoamine Hydrogel Composites: Preparation, Properties, and Preliminary Evaluation as Scaffolds for Human Pluripotent Stem Cell Culturing. *Macromol. Biosci.* **2016**, *16*, 1533–1544. [[CrossRef](#)] [[PubMed](#)]
23. Mauro, N.; Scialabba, C.; Pitarresi, G.; Giammona, G. Enhanced adhesion and in situ photothermal ablation of cancer cells in surface-functionalized electrospun microfiber scaffold with graphene oxide. *Int. J. Pharm.* **2017**, *526*, 167–177. [[CrossRef](#)] [[PubMed](#)]
24. Mauro, N.; Manfredi, A.; Ranucci, E.; Procacci, P.; Laus, M.; Antonioli, D.; Mantovani, C.; Magnaghi, V.; Ferruti, P. Degradable Poly(amidoamine) Hydrogels as Scaffolds for In Vitro Culturing of Peripheral Nervous System Cells. *Macromol. Biosci.* **2013**, *13*, 332–347. [[CrossRef](#)] [[PubMed](#)]
25. Tonna, N.; Bianco, F.; Matteoli, M.; Cagnoli, C.; Antonucci, F.; Manfredi, A.; Mauro, N.; Ranucci, E.; Ferruti, P. A soluble biocompatible guanidine-containing polyamidoamine as promoter of primary brain cell adhesion and in vitro cell culturing. *Sci. Technol. Adv. Mater.* **2014**, *15*, 045007. [[CrossRef](#)] [[PubMed](#)]
26. Ferruti, P.; Mauro, N.; Falciola, L.; Pifferi, V.; Bartoli, C.; Gazzarri, M.; Chiellini, F.; Ranucci, E. Amphoteric, prevalingly cationic L-arginine polymers of poly(amidoamino acid) structure: Synthesis, acid/base properties and preliminary cytocompatibility and cell-permeating characterizations. *Macromol. Biosci.* **2014**, *14*, 390–400. [[CrossRef](#)]
27. Nurunnabi, M.; Parvez, K.; Nafiujjaman, M.; Revuri, V.; Khan, H.A.; Feng, X.; Lee, Y. Bioapplication of graphene oxide derivatives: Drug/gene delivery, imaging, polymeric modification, toxicology, therapeutics and challenges. *RSC Adv.* **2015**, *5*, 42141–42161. [[CrossRef](#)]
28. Bak, T.-Y.; Kook, M.-S.; Jung, S.-C.; Kim, B.-H. Biological Effect of Gas Plasma Treatment on CO₂ Gas Foaming/Salt Leaching Fabricated Porous Polycaprolactone Scaffolds in Bone Tissue Engineering. *J. Nanomater.* **2014**, *2014*, 657542. [[CrossRef](#)]

29. Tunma, S.; Inthanon, K.; Chaiwong, C.; Pumchusak, J.; Wongkham, W.; Boonyawan, D. Improving the attachment and proliferation of umbilical cord mesenchymal stem cells on modified polystyrene by nitrogen-containing plasma. *Cytotechnology* **2013**, *65*, 119–134. [[CrossRef](#)]
30. Lopez, L.C.; Belviso, M.R.; Gristina, R.; Nardulli, M.; d'Agostino, R.; Favia, P. Plasma-Treated Nitrogen-Containing Surfaces for Cell Adhesion: The Role of the Polymeric Substrate. *Plasma Process. Polym.* **2007**, *4*, S402–S405. [[CrossRef](#)]
31. Kumar, A.; Rao, K.M.; Han, S.S. Mechanically viscoelastic nanoreinforced hybrid hydrogels composed of polyacrylamide, sodium carboxymethylcellulose, graphene oxide, and cellulose nanocrystals. *Carbohydr. Polym.* **2018**, *193*, 228–238. [[CrossRef](#)] [[PubMed](#)]
32. Gao, W. The chemistry of graphene oxide. In *Graphene Oxide Reduct; Reduction Recipes, Spectroscopy, and Applications*; Springer: Cham, Switzerland, 2015. [[CrossRef](#)]
33. Zant, E.; Grijpma, D.W. Synthetic Biodegradable Hydrogels with Excellent Mechanical Properties and Good Cell Adhesion Characteristics Obtained by the Combinatorial Synthesis of Photo-Cross-Linked Networks. *Biomacromolecules* **2016**, *17*, 1582–1592. [[CrossRef](#)] [[PubMed](#)]
34. Wei, N.; Peng, X.; Xu, Z. Understanding Water Permeation in Graphene Oxide Membranes. *ACS Appl. Mater. Interfaces* **2014**, *6*, 5877–5883. [[CrossRef](#)] [[PubMed](#)]
35. Menzies, K.L.; Jones, L. The impact of contact angle on the biocompatibility of biomaterials. *Optom. Vis. Sci.* **2010**, *87*, 387–399. [[CrossRef](#)] [[PubMed](#)]
36. Agarwal, M.; Koelling, K.W.; Chalmers, J.J. Characterization of the degradation of polylactic acid polymer in a solid substrate environment. *Biotechnol. Prog.* **1998**, *14*, 517–526. [[CrossRef](#)]
37. Siow, K.S.; Britcher, L.; Kumar, S.; Griesser, H.J. Plasma Methods for the Generation of Chemically Reactive Surfaces for Biomolecule Immobilization and Cell Colonization—A Review. *Plasma Process. Polym.* **2006**, *3*, 392–418. [[CrossRef](#)]
38. Pradhan, S.; Madke, B.; Kabra, P.; Singh, A. Anti-inflammatory and immunomodulatory effects of antibiotics and their use in dermatology. *Indian J. Dermatol.* **2016**, *61*, 469–481. [[CrossRef](#)]
39. Ko, T.-J.; Kim, E.; Nagashima, S.; Oh, K.H.; Lee, K.-R.; Kim, S.; Moon, M. Adhesion behavior of mouse liver cancer cells on nanostructured superhydrophobic and superhydrophilic surfaces. *Soft Matter* **2013**, *9*, 8705–8711. [[CrossRef](#)]
40. Jeong, J.-T.; Choi, M.-K.; Sim, Y.; Lim, J.-T.; Kim, G.-S.; Seong, M.-J.; Hyung, J.-H.; Kim, K.S.; Umar, A.; Lee, S.-K. Effect of graphene oxide ratio on the cell adhesion and growth behavior on a graphene oxide-coated silicon substrate. *Sci. Rep.* **2016**, *6*, 33835. [[CrossRef](#)]
41. Suhaeri, M.; Noh, M.H.; Moon, J.H.; Kim, I.G.; Oh, S.J.; Ha, S.S.; Lee, J.H.; Park, K. Novel skin patch combining human fibroblast-derived matrix and ciprofloxacin for infected wound healing. *Theranostics* **2018**, *8*, 5025–5038. [[CrossRef](#)]
42. Reinke, J.M.; Sorg, H. Wound repair and regeneration. *Eur. Surg. Res.* **2012**, *49*, 35–43. [[CrossRef](#)] [[PubMed](#)]

